The f'/Q Factor in the Relationship Between Inherent and Apparent Optical Properties in a Typical Inland Water (Lake Taihu, China)

Yu Zhang, Lifu Zhang, *Senior Member, IEEE*, Yi Cen, Hongying Zhao, Junsheng Li, and Qingxi Tong

***Abstract*—Water reflectance anisotropy has serious implications for the remote sensing of water surfaces. The f'/Q factor serves as a crucial bridge connecting the inherent and apparent optical properties of turbid water bodies; f'/Q varies not only with angular geometry and inherent optical properties (IOPs), but also with wavelength. However, there was limited research on f'/Q in turbid water bodies. This research conducted preliminary exploration on f'/Q in inland turbid water bodies based on measurements of in-situ multi-angle bidirectionality reflectance, including 17 angles and 251 bands when the solar zenith angle (θ_s) was between 40° and 50°. This study indicated that f'/Q exhibited highly sensitivity in the wavelength range of 690–750 nm with a peak near 727 nm, as well as angular geometry played an important role in the BRDF. The f'/Q varied over the range of 0.13–0.18 sr^{-1}, variation of 0.06 sr^{-1} across different bands, when viewing zenith angle (θ_v) and particle backscattering ratio ($\tilde{b}_{bp}$) were 0 and 0.0183, respectively; higher than the range observed for the ocean (0.08–0.15 sr^{-1}). The variability in f'/Q as a function of wavelength must be accounted for in turbid waters. The f'/Q was correlated with the IOPs in the range of 690–750 nm, with coefficient of determination (R^2) values higher than 0.94 and root mean square error (RMSE) values lower than 0.004. Our findings are of great significance for understanding the relationship between inherent and apparent optical properties in inland water bodies, for BRDF studies, and for improving the accuracy of satellite product retrieval.**

***Index Terms*—Bidirectional reflectance distribution function (BRDF), inland waters, multi-angle reflectance, radiative transfer, remote sensing.**

I. Introduction

REMOTE sensing reflectance (*Rrs*, sr^{-1}. see Table I for primary symbols and definitions used in this paper) provides necessary information about water surfaces and is not isotropic [1], [2], [3]. The bidirectional reflectance distribution function (BRDF) factor f'/Q (if the backscattering coefficient b_b is small with respect to the absorption coefficient a, the coefficient f' is replaced by f) varies not only with angular geometry and inherent optical properties (IOPs), but also with wavelength. Variability in the f'/Q ratio and its influence on ocean color remote sensing have been the focus of several theoretical studies. Morel and Gentili [2] showed that the f'/Q ratio was relatively independent of the solar zenith angle θ_s and satellite viewing angles expected for the moderate resolution imaging spectroradiometer (MODIS) orbit, with $f'/Q = 0.0936$, 0.0944, 0.0929, and 0.0881 (standard deviation is 0.005) for $\lambda = 440$, 500, 565, and 665 nm, respectively. Thus, in various bio-optical algorithms that relate Rrs to IOPs, f'/Q is assumed to be independent of wavelength λ and θ_s for all MODIS wavebands of interest except for 667 nm (e.g., the MODIS semi-analytical chlorophyll algorithm; Carder et al. [4]). Using detailed radiative transfer computations, Morel et al. [5] found that the typical values of the f'/Q ratio are in the range of 0.08–0.15 sr^{-1} (around the mean value 0.11 sr^{-1} reported by Gordon et al. [6]), and established a look up table of the BRDF accounting for Raman scattering and making the particle phase function shape varying with chlorophyll concentration in open ocean waters. This method was adopted by NASA and has become a standard method. However, it works well only with Case 1 waters [7], i.e., not with coastal or inland waters. Tzortziou et al. [8] estimated values of f'/Q that ranged from 0.09 to 0.107 sr^{-1} for the nadir-viewing geometry in the middle region of Chesapeake Bay. The values were very similar to those reported by Morel and Mueller [9], and were not very different from those of Case 1 waters. Lee et al. [10] developed a method for correcting angle effects in water-leaving radiance (L_w) using an IOP-centered approach, which can be applied to oceanic and coastal waters and has been widely used for correcting the BRDF angle.

Previous studies of bidirectional reflectance were restricted to oceanic and coastal waters, including Case 1 and Case 2 waters [5], [10], [11], [12]. Though the BRDF correction achieved in Case 1 and Case 2 waters, the degree of agreement between theoretical computations and measurements of f'/Q variability in turbid inland waters remains unknown. Further studies are needed for turbid inland waters, which are impacted by human activities and have extremely complex apparent optical properties. In particular, the effects of the BRDF on the co-varying of wavelength and angle in turbid inland waters are seldom

Manuscript received 3 July 2023; revised 17 September 2023; accepted 21 September 2023. Date of current version 18 December 2023. This work was supported in part by the National Key Research and Development Program of China under Grant 2022YFF0904403 and in part by the National Natural Science Foundation of China under Grant 42130104. *(Corresponding author: Hongying Zhao.)*

Yu Zhang is with the Aerospace Information Research Institute, Chinese Academy of Sciences, Beijing 100094, China, and also with the University of Chinese Academy of Sciences, Beijing 100049, China (e-mail: zhangyu21g@mails.ucas.ac.cn).

Lifu Zhang, Yi Cen, Junsheng Li, and Qingxi Tong are with the Aerospace Information Research Institute, Chinese Academy of Sciences, Beijing 100094, China (e-mail: zhanglf@radi.ac.cn; cenyi@radi.ac.cn; lijs@radi.ac.cn; tongqx@aircas.ac.cn).

Hongying Zhao is with Peking University, Beijing 100871, China (e-mail: zhaohy@pku.edu.cn).

Digital Object Identifier 10.1109/JSTARS.2023.3321400

TABLE I
SIGNIFICANT SYMBOLS, DEFINITIONS, AND UNIT

Symbol	Definition	Unit
a	Total absorption coefficient	m^{-1}
a_w	Pure water absorption coefficient	m^{-1}
a_{CDOM}	Yellow substance absorption coefficient	m^{-1}
a_p	Particle-absorption coefficient	m^{-1}
b	Total scattering coefficient	m^{-1}
b_b	Backscattering coefficient	m^{-1}
b_{bw}	Backscattering coefficient of water molecules	m^{-1}
b_{bp}	and particles, respectively	m^{-1}
$\tilde{b}_{bp}$	Particle backscattering ratio ($=b_{bp}/b_p$)	–
C_{pg}	Attenuation coefficient of dissolved and particulate constituents	m^{-1}
E_d	Downwelling irradiance	$W\ m^{-2}$
E_u	Upwelling irradiance	$W\ m^{-2}$
f	Ratio of Subsurface irradiance reflectance to the ratio b_b/a	–
f'	Ratio of Subsurface irradiance reflectance to the ratio $b_b/(a+b_b)$	–
L_u	Upwelling radiance	$W\ m^{-2}\ sr^{-1}$
L_w	Water-leaving radiance	$W\ m^{-2}\ sr^{-1}$
n	Refractive index of water	–
Q	Ratio of irradiance to radiance	sr
Rrs	Above-surface remote-sensing	sr^{-1}
R	Irradiance reflectance ($=E_u/E_d$)	–
λ	Wavelength	nm
θs	Solar zenith angle	rad
θv	Viewing zenith angle	rad
$\theta' v$	Viewing nadir angle	rad
φ	Viewing azimuth angle	rad
τ_a	Aerosol optical thickness	–
$\bar{n}$	Average number of collisions	–
$\bar{w}$	Single-scattering albedo	–
W	Wind speed	$m\ s^{-1}$
$\Re$	Divergence factor when radiance enters into air from below the surface	–

addressed due to the difficulty in collecting in situ multiangle data, and the particulate scattering volume function. Most previous studies focused on oceanic and coastal waters, and constructed BRDF models through simulations rather than the collection of in situ bidirectional data. In situ bidirectionality data are rarely measured due to the limitations of instruments measuring bidirectionality and particulate volume scattering functions (VSFs). Water color remote sensing may be influenced by various constituents, such as chlorophyll-a (Chla), total suspended matter (TSM), and colored dissolved organic substances (CDOM). Further studies are needed to determine the variability in BRDF for inland turbid waters, especially in several substances dominated together case 2 waters (T-2). Loisel and Morel [13] studied extreme situations in waters of yellow-substance-dominated (Y-2) and sediment-dominated Case 2 waters (S-2), less distributed in inland waters, and described the effect of θ_s on the bidirectional structure of the upward radiance field. In addition, Y-2, S-2 [13] and T-2 waters in Taihu Lake were compared in terms of their ratio spectral scattering and absorption coefficients (b/a). The b/a spectra are displayed in Fig. 1. T-2 waters was different from S-2 and Y-2 waters, although it had a similar magnitude to S-2 and similar spectral shape to Y-2. It is believed that, in T-2 waters, several substances that are totally dominant. In T-2 waters, the b/a is as

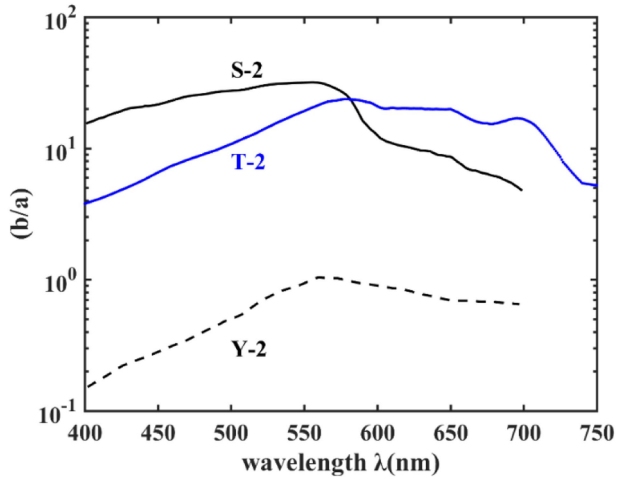

Fig. 1. Spectral values of the b/a ratio for Y-2, S-2, and T-2 waters.

low as 3.78 (single-scattering albedo $\bar{w} = 0.79$) at 400 nm, is maximal (23.67) at 578 nm ($\bar{w} = 0.96$), slightly decreases at 580–650 nm, and strongly decreases at 650–678 nm [due to the increase in the absorption coefficient of phytoplankton (a_{ph})], while there is a slight increase at 678–695 nm with the decrease in a_{ph}. Thus, the bidirectional nature of T-2 waters is likely to be different compared to S-2, Y-2, and Case 1 waters. The upward field tends to become isotropic with increased turbidity and high levels of scattering [9], [13] resulting in f'/Q being less sensitive to the viewing direction. We attempted to determine if the angle geometry tended to be isotropic and had less effect on the BRDF in turbid inland waters. In addition, we investigated whether the independence of the effect of wavelength from f'/Q values in Case 1 waters also applied to inland turbid waters.

In this study, we investigated bidirectional reflectance characteristics in the turbid inland waters of Lake Taihu based on in situ multiangular spectral radiance. Our main objectives were to show the effect of the different phase functions of two particulate backscattering ratios on bidirectional reflectance; analyze and highlight the bidirectional effect of the viewing zenith angle (θ_v), azimuth angle(ϕ), wavelength λ, and their co-variance based on measurements obtained at 17 angles in 251 bands; evaluate the variability in the relationship between f'/Q and IOPs for our measurement geometry. Therefore, the present study has a significant impact in understanding the relationship between inherent and apparent optical properties of inland waters, as well as in enhancing the development of remote sensing algorithms. Although the bottom albedo may have an impact on the upwelling radiant field in inland waters, the high turbidity of Taihu Lake means that this effect is not significant. The effect of winds and aerosol were not considered in our study.

II. METHODS

A. Theoretical Background

The water-leaving radiance $L_w(0^+, \lambda, \Omega, IOP, W, \tau_a)$, is the light intensity per solid angle resulting from absorption and scattering in the water, and contains information regarding the IOPs of water bodies. The $L_w(0^+)$ is related to angular

geometry $\Omega(\text{unit rad})$, water IOPs, and wavelength that can be expressed as follows [5], [6], [14], [15]:

$$Lw\ \left(0^+,\lambda,\theta_s,\theta_v,\varphi,\text{IOP},W,\tau_a\right) = E_d\left(0^+,\lambda,\theta_s,\tau_a\right)\times\Re\left(\theta'_v,W\right) \times\frac{f'\left(\lambda,\theta_s,\text{IOP},W,\tau_a\right)}{Q\left(\lambda,\theta_s,\theta'_v,\varphi,\text{IOP},W,\tau_a\right)}\frac{b_b\left(\lambda\right)}{a\left(\lambda\right)+b_b\left(\lambda\right)} \quad (1)$$

where $E_d(0^+)$ is the downward irradiance just above the surface, and $\Re(\theta'_v, W)$ is a divergence factor that accounts for transmission and reflection effects when radiance enters the air from below the surface. Wind speed (W) has a weak effect on $\Re$ that can be calculated accurately over a wide range of viewing angles using $W = 0$ [16]; normally, it is equal to 0.54. $a(\lambda)$ and $b_b(\lambda)$ are the total absorption and backscattering coefficients at wavelength λ, respectively. The dimensionless coefficient f', which regulates the magnitude of irradiance reflectance, is a complex function of wavelength, θ_s, water IOPs (mainly single scattering albedo and VSF), surface roughness, and aerosol optical thickness (τ_a) [9], [16], [17]. The f' quantity appears through the ratio $R(0^-)$ of upwelling irradiance $E_u(0^-)$ to incident downward irradiance $E_d(0^-)$ (at null depth and just beneath the surface, denoted (0^-)), which is expressed as: $R(0^-) = E_u(0^-)/E_d(0^-) = f'\left(b_b/(a+b_b)\right)$. If b_b is small with respect to a, the coefficient f is used to relate R to the ratio b_b/a and averages about 0.32–0.33 [16]. The global range of variation in f is from about 0.3–0.6 [9]. The bidirectional function Q [14], which is defined as $Q = E_u(0^-)/L_u(0^-,\theta'_v,\varphi)$, is the ratio of upwelling irradiance $E_u(0^-)$ to upwelling radiance $L_u(0^-)$, which gives rise to $L_w(0^+)$ after its emergence. Thus, Q is a bidirectional function with values that generally range from 3 to 6 sr [2] depending on the angular configuration $(\theta_s, \theta'_v, \phi)$, water IOPs (particularly VSF), and environmental factors, including the wavelength, θ_s, nadir angle (θ'_v), ϕ, water IOPs, surface roughness, and τ_a. The θ'_v is the in-water zenith angle of θ_v, which is related to θ through Snell's law ($\sin\ \theta_v = n\sin\theta'_v$, where $n = 1.34$ is the refractive index of seawater). The angular coordinates used in this study refer to MG-96 [3].

The $f'/Q(\text{sr}^{-1})$ describes the bidirectional reflectance when the total backscattering $b_b(\text{m}^{-1})$ is not small compared to the absorption coefficient $a(\text{m}^{-1})$ [15]. The f'/Q factor mainly depends on three variables, i.e., angular geometry, IOPs, and wavelength, with the effect of the W and τ_a being neglected due to their very small influence. Therefore, the multiangular $R_{rs}\ (\lambda,\Omega,\text{IOP})$ could be expressed [6]

$$R_{rs}\ (\lambda,\Omega,\text{IOP}) = \frac{L_w(0^+,\lambda,\Omega,\text{IOP})}{E_d\left(0^+,\lambda,\theta_s\right)}\ . \quad (2)$$

The multiangular R_{rs} processing method [18] used the multiangular spectral radiance data measured above the water surface, including the viewing direction. By rearranging (1) and (2), the multiangular $R_{rs}(\lambda,\Omega,\text{IOP})$ could be expressed in relation to backscattering and absorption coefficients [19]

$$R_{rs}\ (\lambda,\Omega,\text{IOP}) = \Re\left(\theta'_v,W\right)f'/Q(b_b/a+b_b). \quad (3)$$

For turbid waters, the average number of collisions $(\bar{n})$ is important, as it is more directly related to the above parameters [1]. The $\bar{n}$ experienced by photons before they escape from water can be expressed as: $\bar{n} = (1-\bar{w})^{-1}$ or $\bar{n} = 1+(b/a)$. Where $\bar{w}$ is the single-scattering albedo, $\bar{w} = b/(a+b)$, and a and b are the absorption and scattering coefficients, respectively. It should be noted that we used $\bar{n}$ instead of $\bar{w}$ because $\bar{n}$ is unbounded and more intuitive than $\bar{w}$ [13], especially when multiple-scattering is dominant in turbid waters.

TABLE II
RELEVANT OPTICAL INFORMATION OBTAINED AT SAMPLING SITES DURING A TAIHU LAKE CRUISE IN 2012

No.	Year/month	Solar zenith angle [°]	Chla [mg m^{-3}]	TSM [mg L^{-1}]	bp(550) [m^{-1}]	$a_{CDOM}(400)$ [m^{-1}]
1	October 2012	47.4	22.25	120.08	19.51	1.06
2	October 2012	41.3	13.78	86.31	17.89	1.02
3	October 2012	41.6	13.95	46.62	14.12	1.02
4	October 2012	49.2	15.12	38.85	12.72	1.03
7	October 2012	41.2	30.23	40.11	16.31	0.98
8	October 2012	43.6	21.81	35.99	13.78	0.91
9	October 2012	50.0	25.21	37.78	14.88	0.96

Note: The terms $b_b(550)$ and $a_{CDOM}(400)$ are the particles scattering coefficient at 550 nm and the absorption coefficient of dissolved yellow substances at 400 nm, respectively.

B. Data Processing and Calculation of the f'/Q Ratio

The multiangular remote-sensing reflectance $R_{rs}(\lambda,\Omega,\text{IOP})$ was measured using a handheld three-dimensional positioning pole, with measurements made 10 times in every observation direction [18] on cloudless sunny days. The viewing zenith angle θ_v was measured from 0° to 60° at intervals of 15°, and the viewing angle relative to the sun φ were measured from 0° to 145° at intervals of 45°.

Therefore, bidirectionality data was measured including 17 observation directions (θ_v = 0°, 15°, 30°, 45° or 60°; φ = 0°, 45°, 90°, or 135°) and 251 bands (500–750 nm, at an interval of 1 nm) in Taihu, China [18]. Seven stations (see Table II) were used in our study; data from stations 5 and 6 were omitted due to the small variations in θ_s. Some IOPs were measured in the laboratory. The absorption coefficient spectra of CDOM ($a_{\text{CDOM}}(\lambda)$) and beam attenuation coefficient spectra of dissolved and particulate constituents ($C_{pg}(\lambda)$) were measured by ultra-violet-visible spectroscopy (UV2410PC; Shimadzu, Kyoto, Japan) and calculated [20]. The absorption coefficients of total suspended matter($a_p(\lambda)$) and nonalgal particles ($a_{\text{NAP}}(\lambda)$) were measured using a quantitative filter technique [21] and calculated as proposed Cleveland et al. [22]. The absorption coefficient spectra of phytoplankton ($a_{\text{ph}}(\lambda)$) were obtained by subtracting $a_{\text{NAP}}(\lambda)$ from $a_p(\lambda)$, and the scattering coefficient spectra of TSM ($b_p(\lambda)$) were obtained by subtracting $a_p(\lambda)$ and $a_{\text{CDOM}}(\lambda)$ from $C_{pg}(\lambda)$. The TSM and Chla concentrations were also measured. Some IOPs and related data are listed in Table II. The average $a_{\text{CDOM}}(\lambda)$, $a_{\text{NAP}}(\lambda)$, $a_{\text{ph}}(\lambda)$, and $b_p(\lambda)$ spectra of seven sampling sites were shown in Fig. 2.

The spectral total absorption coefficient $a(\lambda)$ was calculated as follows:

$$a\left(\lambda\right) = a_w\ \left(\lambda\right) + a_{\text{CDOM}}\left(\lambda\right) + a_{\text{ph}}\left(\lambda\right) + a_{\text{NAP}}\left(\lambda\right) \quad (4)$$

where $a_w(\lambda)$, $a_{\text{CDOM}}(\lambda)$, $a_{\text{ph}}(\lambda)$, and $a_{\text{NAP}}(\lambda)$ are the absorption coefficients of pure water, CDOM, phytoplankton, and nonalgal

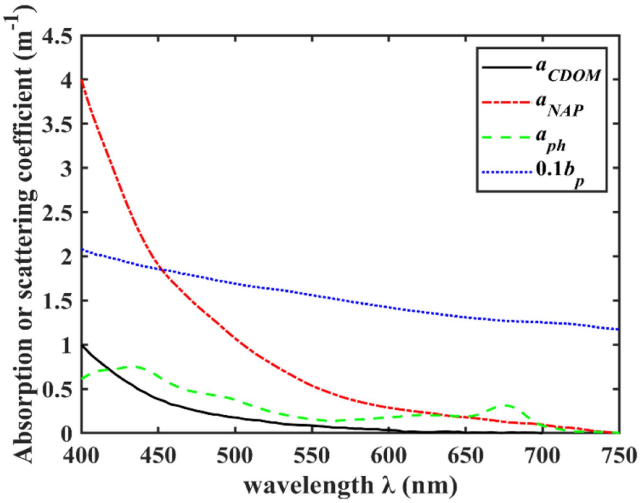

Fig. 2. Average spectral values of $a_{\mathrm{CDOM}}(\lambda)$, $a_{\mathrm{NAP}}(\lambda)$, $a_{\mathrm{ph}}(\lambda)$, and $b_p(\lambda)$ of the seven sampling sites.

particles, respectively. $a_w(\lambda)$ was taken from Pope et al. [23] and Lee et al. [24], and linearly interpolated at intervals of 1 nm.

The angular shape of the particle scattering phase function is not a constant; it varies with particle size and composition [25], [26]. However, there is no reliable method to accurately measure the particle phase function shape; therefore, BRDF values will always be a best-guess estimate at present. Fortunately, recent technological advances have greatly expanded the number of VSFs and more models have been developed [27], [28]. Finally, we selected two different particulate backscattering ratios ($\tilde{b}_{bp}(\lambda)$); one was the commonly used value of 0.0183 from Petzold's integrated volume scattering data, while the other is the 0.013 was obtained by Whitmire et al. [29] using a much larger data set. The particulate backscattering coefficients ($b_{bp}(\lambda)$) were calculated directly as $\tilde{b}_{bp}(\lambda) \times b_p(\lambda)$ for all wavelengths. The spectral total backscattering coefficient $b_b(\lambda)$ was calculated as follows:

$$b_b(\lambda) = b_{bw}(\lambda) + b_{bp}(\lambda) \tag{5}$$

where $b_{bw}(\lambda)$ and $b_{bp}(\lambda)$ are the backscattering coefficients of pure water and total suspended particles, respectively. $b_{bw}(\lambda)$ was taken from Dall'Olmo et al. [30] and linearly interpolated at an interval of 1 nm.

In this study, the effects of W and τ_a were ignored because $W \leq 5$ m/s on the cloudless sunny days that characterized the study period. Based on the definition of R_{rs}, a multiangular $R_{rs}(\lambda, \Omega, \mathrm{IOP})$ was estimated as the ratio of $L_w(0^+, \lambda, \Omega, \mathrm{IOP})$ to the measured $E_d(0^+, \lambda, \theta_s)$ provided by (2). The IOPs (i.e., a, bb) were measured and variability in the quantity $f'/Q(\mathrm{sr}^{-1})$ was estimated according to (3). The time period selected was 10.00 to 14.00. The θ_s ranged from 40°–50°, and we assumed that θ_s was invariant while θ_v and φ changed. Therefore, $f'/Q(\mathrm{sr}^{-1})$ was a function of wavelength, ϕ, θ_v, and IOPs.

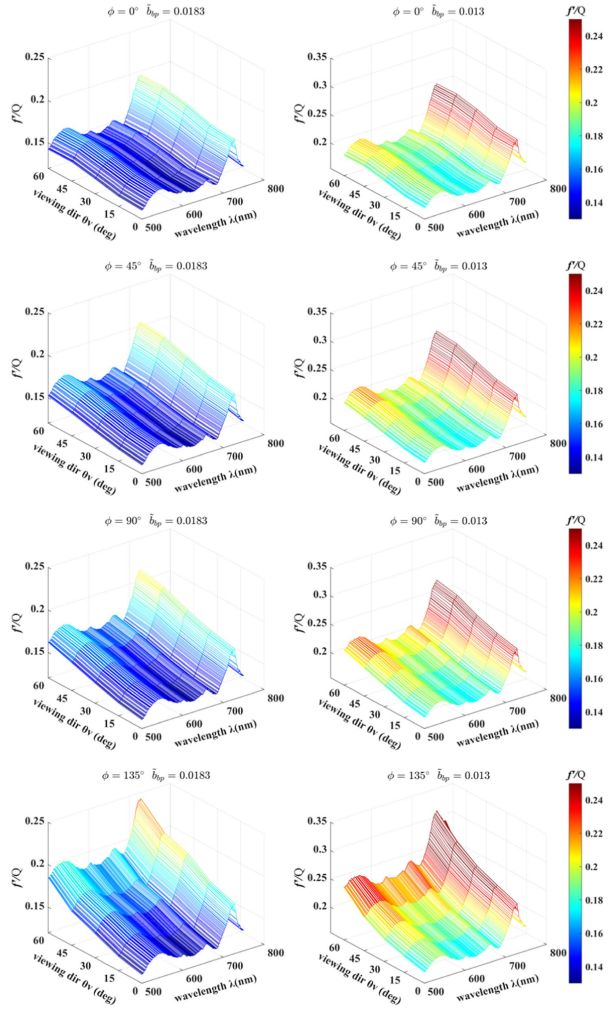

Fig. 3. f'/Q of two particulate backscattering ratios (left: 0.0183, right: 0.013) as a function of viewing direction and wavelength at azimuth angles of 0°, 45°, 90°, and 135° (from top to bottom).

III. Results

A. Selection of the Particle Backscattering Ratios $\tilde{b}_{bp}$

With reference to (3), the BRDF factor f'/Q was calculated as a function of the wavelength and angle geometry (see Fig. 3). The overall range of variation of this quantity was 0.130–0.331 sr^{-1}. Two particle backscattering ratios ($\tilde{b}_{bp}$) value (0.0183 and 0.013) were used to calculate the backscattering coefficient b_b. The backscattering ratios exhibited a similar trend but a diverse range of f'/Q values (see Fig. 3). Larger values of f'/Q were seen when the backscattering ratio was equal to 0.013 (in the range of 0.174–0.331 sr^{-1}), and were in the range of 0.130–0.243 sr^{-1} when applying the commonly used value of 0.0183 derived from Petzold's integrated volume scattering. Therefore, we selected 0.0183 for this research due to the changes in angle and wavelength being like those in Petzold [25].

B. Variations With Viewing Angles and Wavelength

Two-way analysis of variance (ANOVA) was used to determine the statistical significance of bidirectional reflectance

TABLE III
TWO-WAY ANOVA OF f'/Q ACCORDING TO WAVELENGTH (500–750 NM) AND ANGLE GEOMETRY (VIEWING ANGLE OF 0°–60° AND AZIMUTH ANGLE OF 0°–135°)

Source	SS	df	MS	F	P
Wavelengths	0.654	250	0.0026	587.2	0
Angles	0.682	16	0.0426	9561.5	0
Error	0.018	4000	0		
Total	1.354	4266			

Note: SS, DF, and MS Represent the Sum of Squares, Degrees of Freedom, and Mean Square, Respectively.

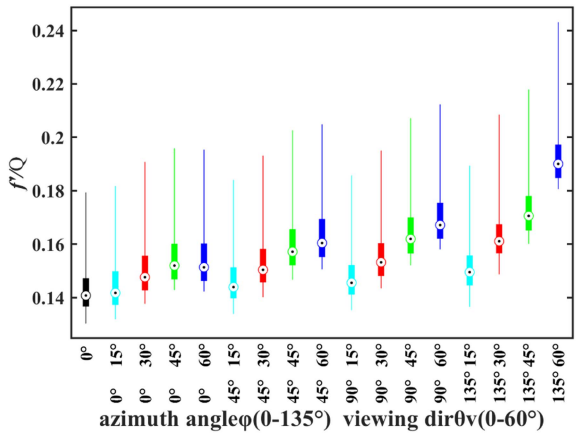

Fig. 4. Summary of f'/Q as a function of azimuth angle ϕ (0°, 45°, 90°, and 135°) and viewing angle θ_v (0°, 15°, 30°, 45°, and 60°) in wavelengths of 400–750 nm.

with variations in wavelength and angle geometry. The ANOVA showed that the impacts of the 251 bands and 17 angles on f'/Q values (see Table III) were significantly different. The value of P was equal to 0, indicating that wavelengths and angles affected the bidirectional reflectance.

The box plot in Fig. 4 shows the distribution of the BRDF factor, f'/Q, across the azimuth and viewing angles for all bands. The box plot depicts the distribution of f'/Q as follows. The box shows the interquartile range (middle 50% of the data), the circle with dots shows the median f'/Q, and the thin lines (whiskers) extending out of the box show the full range of data values (including extreme values). Box plots are useful for visualizing such features. The same line type has the same φ and the same color indicates the same θ_v.

For a viewing angle equal to 0°, f'/Q values were in the range of 0.130–0.179 sr^{-1}; the median was 0.141 sr^{-1}. These values were smaller than for other angles. At a viewing angle θ_v equal to 15°, the f'/Q values increased with increasing ϕ, with median values of 0.142, 0.144, 0.146, and 0.150 sr^{-1} for ϕ of 0°, 45°, 90°, and 135°, respectively. The trends of the other interquartile values were the same, with an increase with increasing ϕ of 0.005–0.007 sr^{-1}. There were no obvious changes when the viewing angle θ_v was $\leq$15° as the ϕ increased from 0° to 145°. However, at a viewing angle of 30°, there were obvious changes as the ϕ increased from 0° to 145°, and especially from 90° to 145°, with an increase of around 0.01 sr^{-1} seen in the f'/Q interquartile values. This change was more obvious when the viewing angle θ_v was 45° or 60°. For example, when the viewing angle was 60°, the median value increased by 0.023 sr^{-1} as

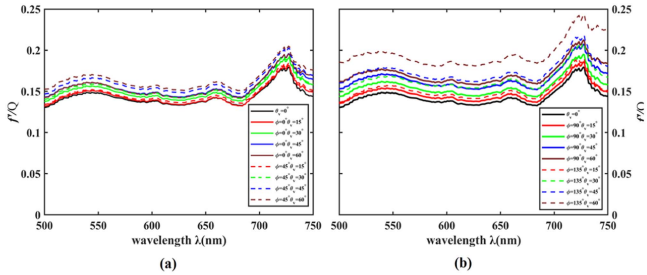

Fig. 5. Spectral values of f'/Q at various angles: (a) $\varphi = 0°$ and 45° and $\theta_v = 0°$, 15°, 45°, and 60°; (b) $\varphi = 90°$ and 135° and $\theta_v = 0°$, 15°, 45°, and 60°.

the ϕ increased from 90° to 145°. The viewing angle had more effect on the f'/Q than the azimuth angle ϕ. With an increase in viewing angle, the f'/Q interquartile values increased for an ϕ of 0°–145°. More importantly, the larger the azimuth angle, the greater effect of viewing angle changes on f'/Q. For example, at an ϕ of 0°, all the interquartile values increased by 0.01 sr^{-1} for viewing angles of 0–60°. However, the interquartile values increased by 0.041–0.054 sr^{-1} at an ϕ equal to 135°. In addition, the change is relatively small in the 0 degrees azimuth.

The overall range of variation of f'/Q with wavelength was 0.130–0.243 sr^{-1} (see Fig. 5). The f'/Q value increased monotonously with wavelength from 500 to 540 nm. There were small changes ($\sim$0.015 sr^{-1}) from 541 to 685 nm. In the range of 690–750 nm, f'/Q initially increased to extreme values and then decreased. The extreme values occurred in the infrared region at 727 nm, which was related to IOPs, absorption and scattering (see Section IV-A).

We evaluated the effect of changes in the main wavelength bands (510, 531, 555, 620, 645, 660, 678, 690, 708, 727, and 740 nm) on the f'/Q. Those bands, including several wavelengths generally used in satellite measurements, have been applied for the retrieval of chlorophyll and sediment concentrations in turbid waters. The f'/Q was very complex result from water inherent optical properties with wavelength. The variations in interquartile values were like those in the mean values. The mean f'/Q value was 0.162 sr^{-1} for the main bands. The f'/Q value increased from 690 to 728 nm and then decreased. There were few differences among the bands. For example, at 531 and 555 nm, the mean value was 0.162 sr^{-1} at both 531 and 555 nm, the minimum value was 0.146 sr^{-1}, the 25% and 75% interquartile values were 0.154 and 0.168 sr^{-1}, respectively, and the median values were 0.1588 and 0.1583 sr^{-1}, respectively. However, there was a slight difference in the maximum values (0.197 and 0.194 sr^{-1}, respectively) when the viewing direction was 60°. we should draw attention to viewing direction that is equal to 60°. The 531 and 555 nm combination was therefore useful for turbid waters retrieval. Furthermore, 510, 645, and 690 nm had equal mean and interquartile values as well expect for the maximum of 510 nm, 0.1896 sr^{-1}, that is bigger than 645 and 690 nm. This is to say the effect of BRDF on them is extremely similar or same. we also can use 510,645, and 690 nm combination to retrieve. In conclusion, 531 and 555 nm combination and 510, 645, and 690 nm combination all can be

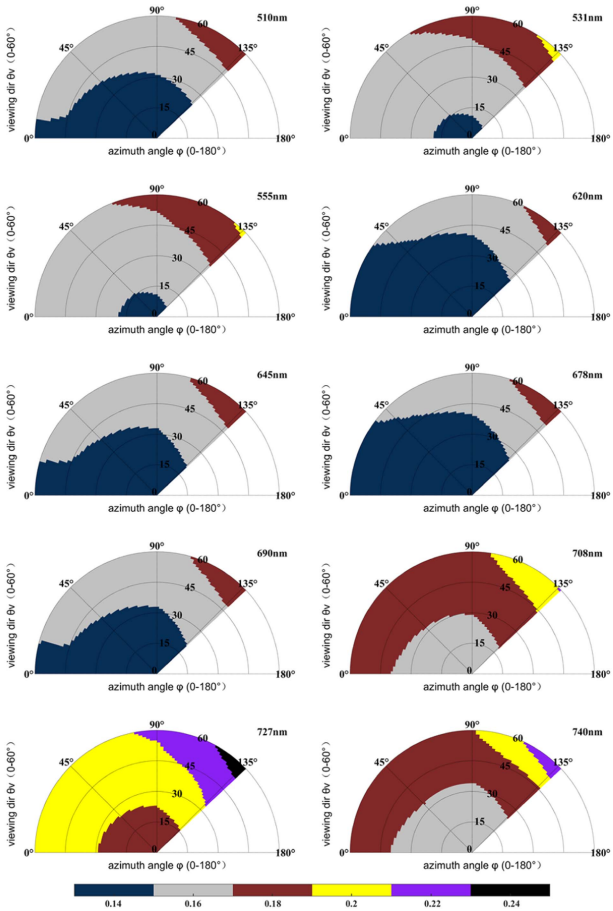

Fig. 6. Polar plots of f'/Q at viewing angles of 0°–60° and azimuth angles of 0°–135°, including the visible and infrared parts of the spectrum. The polar radius represents viewing angles of 0°–60° and the polar angle represents azimuth angles of 0°–135°.

used to retrieve due to the same effect of BRDF on those bands when viewing angle less than 60°.

C. Look-Up Tables of the f'/Q

Data for the selected solar zenith angles between 40° and 50° for Taihu Lake inland waters (see Table II and Fig. 5) were linearly interpolated. The corresponding polar plots of the color encoded f'/Q quantity is also shown (see Fig. 6) for the different wavelengths, used in water color remote sensing studies (510, 531, 555, 620, 645, 678, 690, 708, 727, and 740 nm). The polar radius represents the viewing angle (0°–60°) and the polar angle represents the ϕ (0°–135°). The following observations were made.

1) The f'/Q patterns were largely wavelength dependent in this turbid inland water body, especially at 708, 727, and 740 nm.
2) At the ϕ of 0°, the viewing direction had little effect on the f'/Q at 510, 620, 645, 678, 690, 708, 727, and 740 nm.
3) The viewing angle θ_v had an obvious effect on the f'/Q, which increased with increasing ϕ.
4) Generally, the f'/Q value increased with the viewing angle θ_v and azimuth angle ϕ. More importantly, the effect of the θ_v was greater than the ϕ.
5) For several wavelengths (e.g., 531 and 555 nm, and 510, 620, and 690 nm) f'/Q patterns were highly similar regardless of the angle geometry.

Thus, more attention should be focused on the effect of the f'/Q on turbid inland water bodies, regardless of the angle geometry or wavelength.

Example mean f'/Q values and standard deviation as a function of wavelength, viewing angle, and azimuth angle are provided in Tables IV and V; detailed lookup tables data for other wavelength values are available on request from the authors.

TABLE IV
PART OF THE LOOKUP TABLES CONTAINING MEAN f'/Q VALUES AND STANDARD DEVIATION FROM 510 TO 620 NM FOR TURBID INLAND WATERS (VIEWING ANGLE θV OF 0°–60° AND AZIMUTH ANGLE Φ OF 0°–135°)

Parameter	Wavelength(nm)				
f'/Q	510	531	555	620	645
$\theta_v = 0°$	0.136±0.023	0.146±0.026	0.147±0.027	0.134±0.024	0.137±0.024
$\varphi = 0° \theta_v = 15°$	0.138±0.027	0.149±0.031	0.149±0.033	0.134±0.030	0.138±0.030
$\varphi = 0° \theta_v = 30°$	0.144±0.026	0.154±0.029	0.154±0.030	0.140±0.028	0.144±0.028
$\varphi = 0° \theta_v = 45°$	0.149±0.019	0.159±0.022	0.158±0.024	0.144±0.021	0.148±0.021
$\varphi = 0° \theta_v = 60°$	0.148±0.016	0.159±0.019	0.158±0.021	0.143±0.016	0.147±0.016
$\varphi = 45° \theta_v = 15°$	0.140±0.025	0.150±0.028	0.150±0.029	0.137±0.026	0.140±0.026
$\varphi = 45° \theta_v = 30°$	0.146±0.026	0.157±0.029	0.157±0.030	0.143±0.028	0.146±0.027
$\varphi = 45° \theta_v = 45°$	0.153±0.027	0.164±0.030	0.164±0.031	0.149±0.028	0.153±0.028
$\varphi = 45° \theta_v = 60°$	0.158±0.029	0.168±0.033	0.168±0.034	0.152±0.031	0.156±0.031
$\varphi = 90° \theta_v = 15°$	0.141±0.025	0.152±0.028	0.152±0.028	0.138±0.026	0.142±0.026
$\varphi = 90° \theta_v = 30°$	0.150±0.024	0.160±0.027	0.159±0.028	0.145±0.026	0.149±0.025
$\varphi = 90° \theta_v = 45°$	0.159±0.026	0.169±0.029	0.168±0.029	0.153±0.027	0.157±0.026
$\varphi = 90° \theta_v = 60°$	0.167±0.030	0.175±0.032	0.173±0.032	0.159±0.030	0.163±0.031
$\varphi = 135° \theta_v = 15°$	0.143±0.025	0.154±0.026	0.155±0.026	0.142±0.025	0.146±0.024
$\varphi = 135° \theta_v = 30°$	0.155±0.027	0.166±0.029	0.166±0. 029	0.154±0.028	0.159±0.027
$\varphi = 135° \theta_v = 45°$	0.166±0.033	0.177±0.035	0.176±0.034	0.162±0.034	0.167±0.033
$\varphi = 135° \theta_v = 60°$	0.190±0.041	0.197±0.042	0.194±0.040	0.182±0.043	0.186±0.042

TABLE V
PART OF THE LOOKUP TABLES CONTAINING MEAN f'/Q VALUES AND STANDARD DEVIATION FROM 645 TO 740 NM

Parameter	Wavelength(nm)					
f'/Q	660	678	690	708	728	740
$\theta_v = 0°$	0.143±0.024	0.134±0.018	0.138±0.018	0.158±0.023	0.179±0.026	0.152±0.026
$\varphi = 0° \theta_v = 15°$	0.143±0.030	0.133±0.025	0.138±0.025	0.160±0.031	0.181±0.032	0.157±0.029
$\varphi = 0° \theta_v = 30°$	0.149±0.029	0.139±0.024	0.144±0.024	0.167±0.029	0.190±0.030	0.166±0.028
$\varphi = 0° \theta_v = 45°$	0.153±0.021	0.144±0.017	0.148±0.016	0.172±0.020	0.195±0.019	0.172±0.020
$\varphi = 0° \theta_v = 60°$	0.152±0.016	0.143±0.014	0.147±0.013	0.173±0.016	0.195±0.014	0.175±0.016
$\varphi = 45° \theta_v = 15°$	0.146±0.026	0.137±0.020	0.141±0.020	0.162±0.026	0.183±0.030	0.159±0.029
$\varphi = 45° \theta_v = 30°$	0.152±0.028	0.142±0.022	0.147±0.022	0.169±0.029	0.192±0.033	0.168±0.033
$\varphi = 45° \theta_v = 45°$	0.159±0.028	0.148±0.022	0.153±0.022	0.177±0.029	0.202±0.034	0.178±0.033
$\varphi = 45° \theta_v = 60°$	0.162±0.032	0.152±0.025	0.156±0.026	0.180±0.032	0.204±0.037	0.183±0.037
$\varphi = 90° \theta_v = 15°$	0.147±0.026	0.138±0.019	0.142±0.019	0.163±0.024	0.185±0.027	0.158±0.026
$\varphi = 90° \theta_v = 30°$	0.154±0.026	0.145±0.019	0.149±0.019	0.171±0.023	0.194±0.024	0.167±0.025
$\varphi = 90° \theta_v = 45°$	0.163±0.027	0.154±0.021	0.157±0.021	0.181±0.025	0.206±0.027	0.180±0.027
$\varphi = 90° \theta_v = 60°$	0.170±0.026	0.161±0.025	0.163±0.027	0.186±0.025	0.212±0.030	0.191±0.030
$\varphi = 135° \theta_v = 15°$	0.151±0.025	0.142±0.019	0.146±0.019	0.167±0.023	0.189±0.030	0.160±0.030
$\varphi = 135° \theta_v = 30°$	0.165±0.027	0.154±0.020	0.157±0.020	0.181±0.025	0.208±0.032	0.177±0.032
$\varphi = 135° \theta_v = 45°$	0.174±0.033	0.164±0.026	0.167±0.025	0.191±0.031	0.218±0.037	0.190±0.039
$\varphi = 135° \theta_v = 60°$	0.195±0.043	0.187±0.037	0.187±0.033	0.212±0.038	0.243±0.044	0.230±0.048

IV. DISCUSSION

Large variations of f'/Q were seen according to wavelength (see Fig. 5), different from previous studies [5], [13] which the f'/Q was not highly spectrally sensitive. It is important

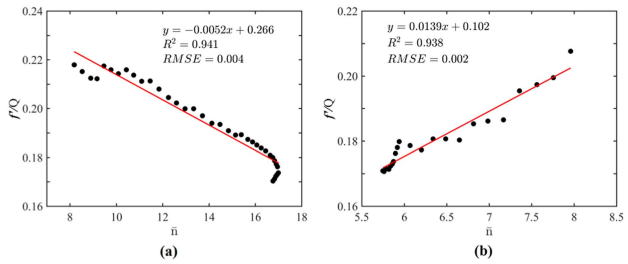

Fig. 7. (a) Scatter plot of f'/Q (45°,135°) and $\bar{n}$ in the range of 690–727 nm. (b) Scatter plot of f'/Q (45°,135°) and $\bar{n}$ in the range of 728–750 nm.

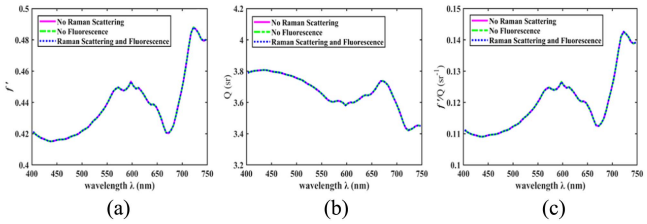

Fig. 8. The spectra of (a) f', (b) Q, and (c) f'/Q were obtained both without considering Raman scattering and fluorescence, as well as including Raman scattering and fluorescence, within the range of 400–750 nm, respectively.

to determine why f'/Q varies with wavelength. The largest changes in the f'/Q values in this study occurred from 690 to 727 nm, and 728 to 750 nm, and may be attributable to average number of collisions $\bar{n}$ and inelastic scattering. In addition, solar zenith angle θ_s is a crucial factor to impact BRDF though the multiangular remote-sensing reflectance was measured maintaining small variations. Therefore, it is necessary to explore the relationships and influences of these three factors on f'/Q .

A. Average Number of Collisions $\bar{n}$ Considerations

The average number of collisions $\bar{n}$ (6), is an intuitively efficient symbol of diffuseness state inside the radiant field, which is in turn directly related to the f'/Q [1]. The f'/Q of viewing angle $\theta_v = 45°$ and azimuth angle $\varphi = 135°$ was used and $\bar{n}$ was analyzed in relation to $f'/Q(45°, 135°)$ (see Fig. 7). Negative correlations between f'/Q and $\bar{n}$ were apparent [see Fig. 7(a)] at wavelengths of 690–727 nm as a result of absorption and scattering, with f'/Q values increased as absorption increased and scattering decreased. At 728–750 nm, there was a positive linear correlation [see Fig. 7(b)] between f'/Q and $\bar{n}$ ($R^2 = 0.938$), with f'/Q increasing with $\bar{n}$. The f'/Q values also increased as absorption increased and scattering decreased. The above results indicate the need to further study the relationship between f'/Q and IOPs.

B. Inelastic Scattering Considerations

The relationship between f'/Q and wavelength is likely influenced by inelastic scattering, primarily involving chlorophyll fluorescence, CDOM, and Raman scattering. The f', Q, and f'/Q values (see Fig. 8) of station 1 were computed to study the impact of inelastic scattering through radiative transfer simulations using the HydroLight 6.0 [31] code. The simulations were conducted with the following input parameters

1) wavelength, λ (100 values, from 400 to 750 nm at an interval of 5 nm);
2) depth: infinite depth;
3) particles ratio, $\tilde{b}_{bp}$: 0.0183;
4) chlorophyll concentration: 22.25 mg m^{-3};
5) mineral particle concentration: 95.88 g m^{-3};
6) CDOM absorption at 440nm: 0.53 m^{-1};
7) Raman scattering coefficient at 488nm: 2.60 × 10^{-4};
8) chlorophyll fluorescence quantum efficiency: 0.02;
9) solar zenith angle: 47.40°;
10) wind speed: 5 m/s;
11) real index of refraction: 1.34;
12) cloud coverage: 0%;
13) airmass type: continental;
14) relative humidity: 80.0%;
15) aerosol optical thickness at 550 nm: 0.261;
16) total ozone: 300.0 Dobson units.

In addition, the IOP models and other input parameters were consistent with Zhang et al. [32] which was focused on the f' factor using He6. The impacts of Raman scattering and fluorescence [31] on the f', Q, and f'/Q were depicted in Fig. 8(a)–(c), respectively. From Fig. 8, it can be observed that inelastic scattering had almost no impact on f', Q, and f'/Q . This may be attributed to the turbidity of the Lake, which masked inelastic scattering due to high-intensity scattering. The results of radiative transfer simulations revealed that the shape of f'/Q closely resembled that of f', with f' and Q exhibiting contrasting characteristics in their variations.

C. Solar Zenith Angle θ_s Considerations

The variation in solar zenith angle within the range of 40°–50° and there is still a maximum difference of 10° among different sites. Its impact on f'/Q are of paramount importance to this study. Therefore, it is essential to use radiative transfer simulations to discuss the effect of θ_s on f'/Q. The other input parameters in Section IV-B remained unchanged, with only the θ_s being altered. The coefficient of variation (CV) was used to express the relative variability of f', Q, and f'/Q in various conditions. The formula for the CV is as follows:

$$\mathrm{CV} = \left(\frac{\sigma}{\mu}\right) \times 100\% \tag{6}$$

where σ and μ are the standard deviation and the mean of data, respectively.

The CV for f'/Q [see Fig. 9(a)] remained below 5.98% and was close to the CV for f' within the solar zenith angle range of 40°–50°, which was lower than the CV for wavelengths [see Fig. 9(b)] greater than 7.50%. It was indicated that the influence of wavelength variation on f'/Q was greater than the solar zenith angle when it was within the range of 40°–50°. Moreover, the CV increased as the angle increased, within the range of 0°–80° for solar zenith angles. The CV for wavelength was at its lowest, approximately 0.79%, at a viewing zenith angle of 10°; and it reached its maximum, approximately 7.84%, at

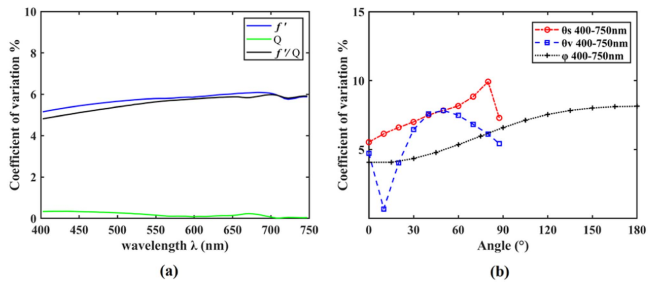

Fig. 9. (a) Coefficients of variation for f', Q, and f'/Q at different wavelengths within the solar zenith angle range of 40°–50° when $\theta_v = 40°, \varphi = 135$. (b) The coefficients of variation of f'/Q at various angles for wavelengths ranging from 400 to 750 nm. Red circle represents θ_s ($\theta_v = 40°$, $\varphi = 135°$); blue square represents θ_v ($\theta_s = 50°, \varphi = 135°$); black plus sign represents φ ($\theta_s = 50°, \theta_v = 40°$).

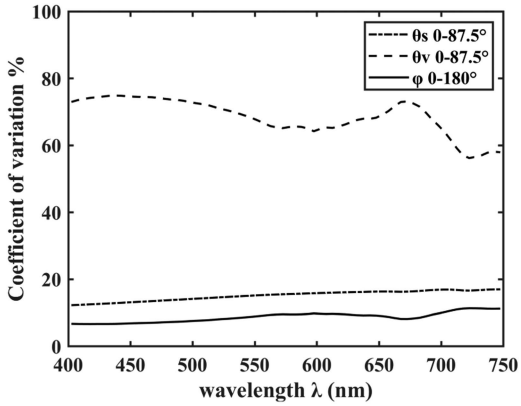

Fig. 10. Coefficients of variation of f'/Q at different wavelengths for solar zenith angle ($\theta_v = 40°, \varphi = 135°$), viewing zenith angle ($\theta_s = 50°, \varphi = 135°$), and viewing azimuth angle ($\theta_s = 50°, \theta_v = 40°$).

50°; and it gradually increased with the increase in azimuth angle. The simulation results were consistent with the in situ results, highlighting that the impact of wavelength on f'/Q was as significant as the influence of angle and should not be overlooked.

Furthermore, the CV for f'/Q with respect to solar zenith angle, viewing zenith angle, and azimuth angle in the 400—750 nm range was calculated (see Fig. 10). The CV for viewing azimuth angle was the smallest ranging from 6.67% to 11.37%, with the CV for solar zenith angle ranging from 12.27% to 17.02%. Notably, the CV for viewing zenith angle was significantly higher than that for solar zenith angle, ranging from 56.19% to 74.89%.

In addition, the particle backscattering ratio $\tilde{b}_{bp}$ is crucial for the study of f'/Q [28], as illustrated in Fig. 3. We modified the input for Part B, changing the value of $\tilde{b}_{bp}$ to range from 0.01 to 0.06 [29], [33], [34], [35], [36] and calculated the CV at different wavelengths, which ranged from 1.98% to 2.91% and was lower than the CV of f'/Q caused by angle and wavelength. More in-depth research is required to explore the relationship between f'/Q and $\tilde{b}_{bp}$ [28], [32].

In this article, we made an uncertainty analysis of $f'/Q\ (573, \theta_v, \varphi)$ according to the relative error in $R_{rs}(573)$ because the relative error in $R_{rs}(\lambda, \theta_v, \varphi)$ is almost constant across the wavelength range, especially in the 500–800 nm. The relative error of $f'/Q\ (573, \theta_v, \varphi)$ was not large and had a slight variation for each observation direction at the seven sample sites. The maximal, minimal and values of these 17 observation directions values were 6.5%, 0.6%, and 3.0%, respectively. And the absorption and backscattering coefficients measuring errors were not included in the estimate of f'/Q error though may significantly modify the relative errors of f'/Q .

V. Conclusion

In this study, the bidirectional reflectance data was measured at 17 angles and 251 bands in an inland turbid lake (Taihu Lake, China). Based on the in situ multiangle bidirectional reflectance data and the calculated f'/Q values, we draw the following conclusions.

1) The f'/Q values varied among wavelength λ, viewing angles θ_v and azimuth angle ϕ in an inland turbid water, and varied over the range of 0.13–0.243 sr^{-1} at $\theta_v = 0°$, higher than the range observed for the ocean (0.08–0.15 sr^{-1}).
2) The f'/Q increased as the θ_v and ϕ increased. The viewing angle θ_v had more effect on the BRDF factor f'/Q than the azimuth angle ϕ; the larger the ϕ, the greater effect of viewing angle changes on the f'/Q . The changes were not obvious when the viewing angle was ≤15°. The variations were greatest when the ϕ and θ_v were 145° and 60°, respectively. The extremely turbid waters are perfectly diffuse scattering bodies, which leads to isotropy [5], [13]. However, an isotropic regime was not reached within the upward field and the angle geometry led to variation in the f'/Q value of about 0.06 sr^{-1}.
3) Wavelength λ also influenced the f'/Q of the L_w in the turbid inland waters, especially in the spectral ranges of 690–750 nm, and the f'/Q ratio was correlated with the IOPs [coefficient of determination (R^2) > 0.94 and RMSE < 0.004).
4) Two particle backscattering ratios (0.0183 and 0.013) exhibited similar trends but produced a diverse range of f'/Q values.
5) Inelastic scattering had a minimal impact on the f'/Q and can be disregarded in Lake Taihu as simulated by Hydrolight.

The bidirectional effects, once computed, can be removed to obtain normalized reflectance or normalized water leaving radiance. The results of this study indicated that lookup tables could be used as a first approximation for f'/Q values in T-2 inland turbid waters at all wavelengths, and could inform the selection of appropriate hyperspectral satellite bands and angles for analyzing turbid inland waters.

Reference

[1] A. Morel and B. Gentili, "Diffuse reflectance of oceanic waters: Its dependence on Sun angle as influenced by the molecular scattering contribution," *Appl. Opt.*, vol. 30, no. 30, Oct. 1991, Art. no. 4427, doi: 10.1364/AO.30.004427.

[2] A. Morel and B. Gentili, "Diffuse reflectance of oceanic waters. II. Bidirectional aspects," *Appl. Opt.*, vol. 32, no. 33, pp. 6864–6879, Nov. 1993, doi: 10.1364/AO.32.006864.
[3] A. Morel and B. Gentili, "Diffuse reflectance of oceanic waters. III. Implication of bidirectionality for the remote-sensing problem," *Appl. Opt.*, vol. 35, no. 24, Aug. 1996, Art. no. 4850, doi: 10.1364/AO.35.004850.
[4] K. Carder, F. R. Chen, Z. P. Lee, S. K. Hawes, and J. P. Cannizaro, "MODIS ocean science team algorithm theoretical basis document ATBD 19 case 2 chlorophyll a, version 7. 30," Coll. Marine Sci., Univ. South Florida, St.Petersburg, FL, USA, Jan. 2003.
[5] A. Morel, D. Antoine, and B. Gentili, "Bidirectional reflectance of oceanic waters: Accounting for Raman emission and varying particle scattering phase function," *Appl. Opt.*, vol. 41, no. 30, Oct. 2002, Art. no. 6289, doi: 10.1364/AO.41.006289.
[6] H. R. Gordon et al., "A semianalytic radiance model of ocean color," *J. Geophysical Res., Atmos.*, vol. 93, no. D9, 1988, Art. no. 10909, doi: 10.1029/JD093iD09p10909.
[7] K. J. Voss, A. Morel, and D. Antoine, "Detailed validation of the bidirectional effect in various case 1 waters for application to ocean color imagery," *Biogeosciences*, vol. 4, no. 5, pp. 781–789, Sep. 2007, doi: 10.5194/bg-4-781-2007.
[8] M. Tzortziou, A. Subramaniam, J. R. Herman, C. L. Gallegos, P. J. Neale, and L. W. Harding, "Remote sensing reflectance and inherent optical properties in the mid Chesapeake Bay," *Estuarine, Coastal Shelf Sci.*, vol. 72, nos. 1/2, pp. 16–32, Mar. 2007, doi: 10.1016/j.ecss.2006.09.018.
[9] A. Morel and J. L. Mueller, "Normalized water-leaving radiance and remote sensing reflectance: Bidirectional reflectance and other factors," Ocean Optics Protocol Satellite Ocean Color Sensor Validation, Revision, Vol. 3, Jan. 2002, pp. 183–210.
[10] Z. P. Lee et al., "An inherent-optical-property-centered approach to correct the angular effects in water-leaving radiance," *Appl. Opt.*, vol. 50, no. 19, Jul. 2011, Art. no. 3155, doi: 10.1364/AO.50.003155.
[11] G. Zibordi and J.-F. Berthon, "Relationships between Q -factor and seawater optical properties in a coastal region," *Limnol. Oceanogr.*, vol. 46, no. 5, pp. 1130–1140, Jul. 2001, doi: 10.4319/lo.2001.46.5.1130.
[12] S. Hlaing et al., "Assessment of a bidirectional reflectance distribution correction of above-water and satellite water-leaving radiance in coastal waters," *Appl. Opt.*, vol. 51, no. 2, pp. 220–237, Jan. 2012, doi: 10.1364/AO.51.000220.
[13] H. Loisel and A. Morel, "Non-isotropy of the upward radiance field in typical coastal (case 2) waters," *Int. J. Remote Sens.*, vol. 22, nos. 2/3, pp. 275–295, Jan. 2001, doi: 10.1080/014311601449934.
[14] R. W. Austin, "The remote sensing of spectral radiance from below the ocean surface," 1974, Accessed: Feb. 08, 2023. [Online]. Available: https://www.semanticscholar.org/paper/The-remote-sensing-of-spectral-radiance-from-below-Austin/98e96eca2a21b9897a5f38f9ea793ad066fc6489
[15] H. R. Gordon, O. B. Brown, and M. M. Jacobs, "Computed relationships between the inherent and apparent optical properties of a flat homogeneous ocean," *Appl. Opt.*, vol. 14, no. 2, pp. 417–427, Feb. 1975, doi: 10.1364/AO.14.000417.
[16] H. R. Gordon, "Normalized water-leaving radiance: Revisiting the influence of surface roughness," *Appl. Opt.*, vol. 44, no. 2, pp. 241–248, Jan. 2005, doi: 10.1364/AO.44.000241.
[17] J. T. O. Kirk, "Dependence of relationship between inherent and apparent optical properties of water on solar altitude," *Limnol. Oceanogr.*, vol. 29, no. 2, pp. 350–356, 1984, doi: 10.4319/lo.1984.29.2.0350.
[18] J. Li, Q. Shen, B. Zhang, F. Zhang, and H. Zhang, "Measurements and analysis of *in situ* multi-angle reflectance of turbid inland water: A case study in Meiliang Bay, Taihu Lake, China," *Int. J. Remote Sens.*, vol. 35, no. 13, pp. 5167–5185, Jul. 2014, doi: 10.1080/01431161.2014.935832.
[19] Z. Lee, K. L. Carder, S. K. Hawes, R. G. Steward, T. G. Peacock, and C. O. Davis, "Model for the interpretation of hyperspectral remote-sensing reflectance," *Appl. Opt.*, vol. 33, no. 24, Aug. 1994, Art. no. 5721, doi: 10.1364/AO.33.005721.
[20] A. Bricaud, A. Morel, and L. Prieur, "Absorption by dissolved organic matter of the sea (yellow substance) in the UV and visible domains," *Limnol. Oceanogr.*, vol. 26, no. 1, pp. 43–53, 1981, doi: 10.4319/lo.1981.26.1.0043.
[21] B. G. Mitchell, "Algorithms for determining the absorption coefficient for aquatic particulates using the quantitative filter technique," in *Proc. 10th Ocean Opt.*, 1990, vol. 1302, pp. 137–148, doi: 10.1117/12.21440.
[22] "Quantifying absorption by aquatic particles: A multiple scattering correction for glass-fiber filters - Cleveland - 1993 - limnology and oceanography–Wiley online library," 2023, Accessed: Apr. 15, 2023. [Online]. Available: https://aslopubs.onlinelibrary.wiley.com/doi/10.4319/lo.1993.38.6.1321
[23] R. M. Pope and E. S. Fry, "Absorption spectrum (380–700 nm) of pure water. II. Integrating cavity measurements," *Appl. Opt.*, vol. 36, no. 33, Nov. 1997, Art. no. 8710, doi: 10.1364/AO.36.008710.
[24] Z. Lee, J. Wei, K. Voss, M. Lewis, A. Bricaud, and Y. Huot, "Hyperspectral absorption coefficient of 'pure' seawater in the range of 350–550 nm inverted from remote sensing reflectance," *Appl. Opt.*, vol. 54, no. 3, pp. 546–558, Jan. 2015, doi: 10.1364/AO.54.000546.
[25] T. J. Petzold, "Volume scattering functions for selected ocean waters," Defense Tech. Inf. Center, Fort Belvoir, VA, USA, Oct. 1972. doi: 10.21236/AD0753474.
[26] M. E. Lee and M. R. Lewis, "A new method for the measurement of the optical volume scattering function in the upper ocean," *J. Atmospheric Ocean. Technol.*, vol. 20, no. 4, pp. 563–571, Apr. 2003, doi: 10.1175/1520-0426.
[27] X. Zhang, Y. Huot, D. J. Gray, A. Weidemann, and W. J. Rhea, "Biogeochemical origins of particles obtained from the inversion of the volume scattering function and spectral absorption in coastal waters," *Biogeosciences*, vol. 10, no. 9, pp. 6029–6043, Sep. 2013, doi: 10.5194/bg-10-6029-2013.
[28] S. He, X. Zhang, Y. Xiong, and D. Gray, "A bidirectional subsurface remote sensing reflectance model explicitly accounting for particle backscattering shapes," *J. Geophysical Res., Oceans*, vol. 122, no. 11, pp. 8614–8626, Nov. 2017, doi: 10.1002/2017JC013313.
[29] A. L. Whitmire, E. Boss, T. J. Cowles, and W. S. Pegau, "Spectral variability of the particulate backscattering ratio," *Opt. Express*, vol. 15, no. 11, 2007, Art. no. 7019, doi: 10.1364/OE.15.007019.
[30] G. Dall'Olmo and A. A. Gitelson, "Effect of bio-optical parameter variability and uncertainties in reflectance measurements on the remote estimation of chlorophyll-a concentration in turbid productive waters: Modeling results," *Appl. Opt.*, vol. 45, no. 15, May 2006, Art. no. 3577, doi: 10.1364/AO.45.003577.
[31] J. D. Hedley and C. D. Mobley, "HYDROLIGHT 6.0 ECOLIGHT 6.0," p. 139, Dec. 2019. [Online]. Available: https://mail.oceanopticsbook.info/packages/iws_l2h/conversion/files/HE60TechDoc_2019_12_02.pdf
[32] Y. Zhang, L. Zhang, C. Huang, Y. Cen, and Q. Tong, "Dependence of the bidirectional reflectance distribution function factor f' on the particulate backscattering ratio in an Inland Lake," *Remote Sens.*, vol. 15, no. 13, Jul. 2023, Art. no. 3392, doi: 10.3390/rs15133392.
[33] E. Boss, "Particulate backscattering ratio at LEO 15 and its use to study particle composition and distribution," *J. Geophysical Res., Oceans*, vol. 109, no. C1, 2004, Art. no. C01014, doi: 10.1029/2002JC001514.
[34] H. Loisel, X. Mériaux, J.-F. Berthon, and A. Poteau, "Investigation of the optical backscattering to scattering ratio of marine particles in relation to their biogeochemical composition in the eastern English Channel and southern North Sea," *Limnol. Oceanogr.*, vol. 52, no. 2, pp. 739–752, Mar. 2007, doi: 10.4319/lo.2007.52.2.0739.
[35] H. R. Gordon et al., "Spectra of particulate backscattering in natural waters," *Opt. Express*, vol. 17, no. 18, Aug. 2009, Art. no. 16192, doi: 10.1364/OE.17.016192.
[36] M. Kheireddine, R. J. W. Brewin, M. Ouhssain, and B. H. Jones, "Particulate scattering and backscattering in relation to the nature of particles in the Red Sea," *J. Geophysical Res., Oceans*, vol. 126, no. 4, Apr. 2021, Art. no. e2020JC016610, doi: 10.1029/2020JC016610.

Yu Zhang received the bachelor's degree in ocean technology from the Dalian Ocean University, Dalian, China, in 2016, and the master's degree in physical oceanography from the State Key Laboratory of Satellite Ocean Environment Dynamics, Second Institute of Oceanography, Ministry of Natural Resources, Hangzhou, China, in 2020. She is currently working toward the Ph.D. degree in cartography and geographic information system with the National Engineering Laboratory for Satellite Remote Sensing Applications, Aerospace Information Research Institute, Chinese Academy of Sciences, Beijing, China.

Her research interests include remote sensing and bidirectional reflectance distribution function and Radiative Transfer model of inland waters.

Lifu Zhang (Senior Member, IEEE) received the B.E. degree in photogrammetry and remote sensing from the Department of Airborne Photogrammetry and Remote Sensing, Wuhan Technical University of Surveying and Mapping, Wuhan, China, in 1992, the M.E. degree in photogrammetry and remote sensing from the State Key Laboratory of Information Engineering in Surveying, Mapping and Remote Sensing, Wuhan Technical University of Surveying and Mapping, in 2000, and the Ph.D. degree in photogrammetry and remote sensing from the State Key Laboratory of Information Engineering in Surveying, Mapping, and Remote Sensing, Wuhan University, Wuhan, in 2005.

He is currently a Professor with the Aerospace Information Research Institute, Chinese Academy of Sciences, Beijing, China. His research interests include hyperspectral remote sensing and remote sensing of inland waters.

Dr. Zhang is a member of International Society for Optical Engineering (SPIE), the Academy of Space Science of China, and the Chinese National Committee of the International Society for Digital Earth (CNISDE). He is also the Vice-Chairperson of the Hyperspectral Earth Observation Committee, CNISDE, and a Standing Committeeman of the Expert Committee of the China Association of Remote Sensing Applications.

Yi Cen received the Ph.D. degree in photogrammetry and remote sensing from the State Key Laboratory of Information Engineering in Survey, Mapping and Remote Sensing, Wuhan University, Wuhan, China, in 2008.

Since 2014, she has been an Associate Research fellow in the Aerospace Information Research Institute, Chinese Academy of Sciences, Beijing, China. Her major research interests include hyperspectral remote sensing application, emphasis on environmental monitoring, carbon circle, and greenhouse gases.

Hongying Zhao received the Ph.D. degree in computer vision from the Chinese Academy of Sciences, Beijing, China, in 2002.

She is currently an Associate Professor with the Institute of Remote Sensing and Geographical Information System, Peking University, Beijing, China. Her research interests include remote sensing imaging, processing and application and UAV aeronautical remote sensing technology.

Junsheng Li received the Ph.D. degree in remote sensing science from the Institute of Remote Sensing Applications, Chinese Academy of Sciences, Beijing, China, in 2007.

He is currently a Professor with the Aerospace Information Research Institute, Chinese Academy of Sciences. His research interests include water color remote sensing and remote sensing of inland waters, including atmospheric correction, eutrophic state assessment, and water clarity estimation.

Qingxi Tong received the B.S. degree in agrometeorology from Odessa of Hydro Meteorological Institute, Odessa, Ukraine, in 1961.

He has been engaged in the study on the development and application of remote sensing since the beginning of 1970. He is currently the Chief Scientist in a cooperation project of the National Remote Sensing Center of China (NRSCC) and the Surrey Satellite Technology Limited (SSTL), Guildford, U.K., for the development of a small satellite. As a result, a high-performance small satellite named "Beijing-1" has been launched and successfully operated. He is one of the Principal Scientists in remote sensing in China. He has made outstanding contribution in the development of remote sensing technology and applications, particularly in the development of airborne remote sensing system, and in the study of remote sensing spectral properties of Earth resources and environments.

Prof. Tong was the recipient of the National Prizes for Progress of Science and Technology and the Chinese Academy of Sciences (CAS) Prize for Progress of Science and Technology many times due to his achievements. He also received the Achievement for International Remote Sensing Science and Technology by the SPIE in 2002. He is an Associate Editor of *Journal of Remote Sensing*, and an Editorial Committeeman of *Chinese Journal of Space Science*. He is also active in the international cooperation. He was elected as a member of CAS and an Academician of the International Eurasian Academy of Sciences in 1997. He serves as the Chairman of the Expert Committee of NRSCC, and the Ministry of Science and Technology of China.